

Theory of Transient Excited State Absorptions in Solid Pentacene with Implications for Singlet Fission

Souratosh Khan

Department of Physics, University of Arizona Tucson, AZ 85721

Sumit Mazumdar

Department of Physics, University of Arizona

*Department of Chemistry and Biochemistry, University of Arizona and
College of Optical Sciences, University of Arizona*

(Dated: July 29, 2022)

Abstract

We report the first theoretical calculations of excited state absorptions (ESAs) from the singlet and triplet excitons, as well as the key intermediate in the singlet fission (SF) process, the spin singlet multiexciton triplet-triplet state, for solid pentacene with herringbone crystal structure. Our goal is to compare theoretical results against ultrafast transient photoinduced absorption (PA) measurements and their interpretations, which have remained controversial. We show that the elusive triplet-triplet state absorbs both in the visible and near infrared (NIR), at or close to the PA energies assigned to the free triplet exciton. In contrast, the triplet PA has nearly vanishing oscillator strength in the NIR within the rigid herringbone structure. Observable oscillator strength for NIR triplet PA requires photoinduced enhancement of coupling between a pair of neighboring pentacene molecules that confers significant charge-transfer (CT) character to the triplet exciton. We discuss the implication of our results for efficient SF in pentacene and related materials.

The photophysics of pentacene has been of strong interest for decades. In recent years, it is being intensively studied as a material in which SF is nearly 100% efficient^{1,2}. In principle each triplet exciton T_1 generated by SF can undergo charge dissociation at the donor-acceptor interface of an organic heterostructure, doubling the photoconductivity expected from the dissociation of the singlet exciton S_1 . SF-driven enhancement of performance has been found in pentacene-C₆₀ solar cells^{3,4}. These observations have led to a flurry of experimental^{2,5–13} and theoretical^{14–23} research on pentacene and its derivatives.

Although the thermodynamic requirement for SF, $E(S_1) \geq 2 \times E(T_1)$, where $E(\dots)$ is the energy of a state, is met widely, relatively few organic molecular systems actually exhibit efficient SF. Recent research has therefore focused on elucidating the mechanism of SF, in particular, on determining the roles of the intermediates, and that of materials morphology. Experimental ultrafast transient absorption studies performed on pentacene and bis(triisopropylsilyl ethynyl) (TIPS) pentacene, in the solid state (polycrystalline films)^{5–7,9–12} or as concentrated solutions¹³, have established that, (i) a triplet-triplet double excitation ${}^1(TT)_1$ is a key intermediate state in SF^{8,11,12,14,18,20,24–27} (here the superscript refers to spin multiplicity, and the subscript indicates that it is lowest triplet-triplet state), and (ii) the ${}^1(TT)_1$ state consists of two spin triplet excitations on neighboring molecules, whose spin angular momenta are quantum-entangled to give overall spin zero. Beyond these, however, uncertainties remain.

Experimental detection of SF by time-resolved spectroscopy requires the observation of, (i) instantaneous pump-induced appearance of singlet $S_1 \rightarrow S_N$ PA (here S_N are higher singlet excitations) (ii) paired decay of the singlet PA and the rise of triplet $T_1 \rightarrow T_N$ PA which persists to long times. While these observations were claimed in early measurements on pentacene films⁵, they are not considered conclusive as the measurements were in the visible range of the electromagnetic spectrum, where singlet and triplet PAs are overlapping. More recent transient absorption studies^{9,13} have assigned a broad PA at ~ 750 nm–950 nm to triplet PA $T_1 \rightarrow T_2$. Although the growth of this NIR PA is concomitant with the decay of the singlet PA^{9,13}, there are disagreements^{14,18} over this assignment. First, experimentally, the longest wavelength at which monomer triplet PA is found is at 505 nm²⁸; this observation is in agreement with theoretical calculations^{29,30} that we have confirmed here. Second, it has been speculated⁸ that the PA in the NIR is from the ${}^1(TT)_1$ rather than free T_1 . Pensack *et al.* have recently claimed overlapping PAs from T_1 and ${}^1(TT)_1$, in both NIR and the visible¹².

Conversely, Herz *et al.*, based on 3-beam pump-depletion-probe experiment, assign the NIR PA to both ${}^1(\text{TT})_1$ and T_1 , and the visible PA at 500-550 nm to $\text{T}_1 \rightarrow \text{T}_3$ alone¹⁰. Clearly, the elucidation of the mechanism of SF in pentacene, requires credible calculations of ESAs from all relevant states.

In the present work we report precise calculations of ESAs from S_1 , T_1 and ${}^1(\text{TT})_1$ in pentacene in the solid state. Our results allow direct comparisons of theory against experiments, and lead to new insight to SF in pentacene. We have performed multiple reference singles and doubles configuration interaction (MRSDCI)^{23,30,31} (see Methods) calculations of ground and excited states of dimers of pentacene molecules in the herringbone lattice, within the *extended* Pariser-Parr-Pople (PPP) Hamiltonian²³. The π -electron only PPP Hamiltonian^{32,33} allows incorporating CI with up to quadruple excitations from the Hartree-Fock (HF) ground state of the pentacene dimer, which is essential for obtaining precise theoretical description of the multiexciton ${}^1(\text{TT})_1$ state³¹, and more importantly, of ESA from the ${}^1(\text{TT})_1$ to even higher energy states. The extended PPP Hamiltonian is written as,

$$H_{\text{PPP}} = H_{\text{intra}} + H_{\text{inter}} , \quad (1)$$

$$H_{\text{intra}} = \sum_{\mu, \langle ij \rangle, \sigma} t_{ij}^\mu (\hat{c}_{\mu i \sigma}^\dagger \hat{c}_{\mu j \sigma} + \hat{c}_{\mu j \sigma}^\dagger \hat{c}_{\mu i \sigma}) + U \sum_{\mu, i} \hat{n}_{\mu i \uparrow} \hat{n}_{\mu i \downarrow} + \sum_{\mu, i < j} V_{ij} (\hat{n}_{\mu i} - 1) (\hat{n}_{\mu j} - 1) \quad (2)$$

$$H_{\text{inter}} = \sum_{\mu \neq \mu', ij, \sigma} t_{ij}^\perp (\hat{c}_{\mu i \sigma}^\dagger \hat{c}_{\mu' j \sigma} + \hat{c}_{\mu' j \sigma}^\dagger \hat{c}_{\mu i \sigma}) + \frac{1}{2} \sum_{\mu \neq \mu', ij} V_{ij}^\perp (\hat{n}_{\mu i} - 1) (\hat{n}_{\mu' j} - 1) , \quad (3)$$

where H_{intra} and H_{inter} describe intra- and intermolecular interactions, $\hat{c}_{\mu i \sigma}^\dagger$ creates a π -electron of spin σ on carbon (C) atom i belonging to molecule μ , $\hat{n}_{\mu i \sigma} = \hat{c}_{\mu i \sigma}^\dagger \hat{c}_{\mu i \sigma}$ is the number of electrons of spin σ on atom i within chromophore μ , and $\hat{n}_{\mu i} = \sum_{\sigma} \hat{n}_{\mu i \sigma}$. The intramolecular hopping integrals t_{ij}^μ are between nearest neighbor C atoms i and j , U is the Coulomb repulsion between two electrons occupying the same atomic p_z orbital, V_{ij} and V_{ij}^\perp are the long range interatomic intra- and intermolecular Coulomb interactions, respectively. We choose $t_{ij}^\mu = -2.4(-2.2)$ eV for the peripheral (internal) bonds of pentacene²³, and obtain the intermolecular hopping integrals between C atoms i and j separated by distance d_{ij} by adjusting β in the expression^{23,34}

$$t_{ij}^\perp = \beta \exp[(d_{\text{min}} - d_{ij})/\delta] , \quad (4)$$

where d_{min} is taken to be the sum of van der Waals radii of two C atoms, and $\delta = 0.045$ nm³⁴. We choose $\beta = -0.2$ to -0.3 eV. With these β , t_{ij}^\perp beyond the nearest neighbor (-0.13 to -0.195 eV) and next nearest neighbor (-0.07 to -0.105 eV) are insignificant (see Supplementary Information).

The intramolecular intersite Coulomb parameters are obtained from the expression $V_{ij} = U/\kappa\sqrt{1 + 0.6117R_{ij}^2}$, where R_{ij} is the distance in Å between C atoms i and j and κ is an effective dielectric constant³⁵. $U = 11.26$ eV and $\kappa = 1$ correspond to the Ohno parameters for the PPP model³⁶. Nearly quantitative fits to the optical absorption spectra of a large number of π -conjugated systems have been obtained with smaller U (8.0 eV) and larger κ (2.0)^{35,37}. More recent theoretical works suggest smaller³⁸ U and κ . We have performed calculations for the narrow range of parameters $U = 6.0 - 8.0$ eV and $\kappa = 1.3 - 2.0$. We have used the same functional form for V_{ij}^\perp with the same κ as for V_{ij} ²³. Excellent fits to molecular singlet and triplet energies, as well as to the ground state absorption spectrum for the herringbone film are obtained with our parametrizations of H_{intra} and H_{inter} (see below).

Results

Monomer singlet and triplet excited states. The best fits to S_1 and T_1 energies are with $U = 6.0$ eV, $\kappa = 1.8$. For this parameter set our calculated $E(S_1) = 2.09$ eV and $E(T_1) = 0.93$ eV, to be compared against experimental $E(S_1) = 2.15$ eV²⁸ and $E(T_1) = 0.86 - 0.95$ eV^{39,40}. The monomer $T_1 \rightarrow T_3$ excitation energy is 2.46 eV²⁸. The calculated $T_1 \rightarrow T_3$ energy is 2.14 eV for $U = 6.0$ eV, $\kappa = 1.8$. From trial and error we found $T_1 \rightarrow T_3$ excitation energy of 2.46 eV for $U = 7.7$ eV and $\kappa = 1.3$. In the following we therefore report singlet ESA spectra for $U = 6.0$ eV, $\kappa = 1.8$, and the triplet and triplet-triplet ESA spectra for $U = 7.7$ eV and $\kappa = 1.3$. This is only for comparisons to the experimental PA spectra. As we show in the Supplementary Information, the difference in the ESA spectra between the two sets of parameters is small, with $U = 6.0$ eV, $\kappa = 1.8$ giving slightly redshifted triplet ESAs.

The herringbone structure: intra- versus intermolecular excitations.

Singlet ground and excited state absorptions. In Fig. 1(a) we have shown the herringbone structure for the pentacene crystal. Our calculations are for the dimer of molecules indicated in the figure, where we have defined our axes, intermolecular separation and dihedral

angle^{41,42}. The very weak coupling between next nearest neighbor molecules has no effect on the calculated absorption spectrum²³. In Fig. 1(b) we have shown our calculated ground state absorption spectra for $\beta = -0.2$ and -0.3 eV for the dimer of Fig. 1(a) superimposed on the low temperature experimental absorption spectrum⁹. The calculated spectra are obtained from diagonalization of the MRSDCI Hamiltonian matrices alone, and no adjustment of energies were done. The agreement between the calculated and the experimental absorption spectra are excellent. We are able to reproduce the Davydov splitting almost quantitatively; we show in the Supplementary Information that $|\beta| > 0.3$ eV is unrealistic. Our use of the purely electronic Hamiltonian does not imply absence of vibronic coupling⁴³, but indicates that the dominant interactions have been largely included in Eq.1.

Our basis functions are products of many-electron configurations on the individual pentacene molecules that constitute the dimer, within the molecular orbital (MO) description (see Methods)^{23,44}. Each eigenstate is a quantum-mechanical superposition of these product configurations, which can not only be classified as single, double, etc. excitations, but also as intramolecular Frenkel, intermolecular CT or TT. This allows physical characterizations of all eigenstates in terms of their most dominant configurations. In Fig. 1(c) we have shown the dominant many-electron configurations and their coefficients in the normalized wavefunctions for the three final states of the ground state absorption spectrum of Fig. 1(b) for $\beta = -0.2$ eV (the wavefunctions are almost indistinguishable for $\beta = -0.3$ eV, see Supplementary Information), as well as the final states of singlet ESA from the lowest of the three. We have labeled the optical singlet excitons as S_0S_1 for brevity, but they are actually superpositions of S_0S_1 and S_1S_0 . We have also adopted the same convention for all other dimer excited states. Here and below, we retain only configurations with coefficients larger than 0.14 (terms with smaller coefficients are included for special cases). It is emphasized that although the dominant terms involve only single and double excitations across the frontier MOs, the complete wavefunctions have components up to quadruple excitations and across MOs removed far from the chemical potential. The last column in Fig. 1(b) gives the extent of CT character of the complete wavefunction.

As seen in Fig. 1(c), the two S_0S_1 excitations at the lowest and highest energies have strong CT components, while the relatively weaker absorption at intermediate energy is predominantly Frenkel in character. The determination of the lowest S_0S_1 as $\sim 50\%$ CT agrees with previous theoretical work^{19,23}.

Experimentally, singlet PA is seen both in the visible^{5,9} and in the IR^{6,12,13}. In Fig. 1(d) we have shown the calculated ESA from the lowest S_0S_1 to S_0S_2 and S_0S_3 , both in the IR. The inset shows the calculated ESA from S_1 in the monomer (see inset Fig. 1(d)). We find two distinct ESAs in the IR in the herringbone structure, in agreement with experiments on TIPS-pentacene in solution¹³ and in a related compound in the solid state¹², but in contrast to the single ESA in the IR in the monomer. As seen from their wavefunctions ESAs to S_0S_2 and S_0S_3 result from dipole-allowed excitations of the Frenkel and CT components of S_0S_1 , respectively. The absence of a CT component to S_0S_1 in the monomer precludes the PA to S_0S_3 . The nearly equal strengths of the two ESAs in the IR are due to the nearly equal contributions by the Frenkel and CT components to the lowest S_0S_1 .

Triplet and triplet-triplet wavefunctions and ESAs. We write the triplet states also as products of dimer states. Fig. 2(a) shows our calculated triplet ESA from S_0T_1 within the herringbone structure. The strong ESA in the visible occurs at a wavelength close to where monomer triplet PA is observed²⁸. The very weak strengths of the ESAs in the NIR disagrees with the assignment of experimental PA in this region to the triplet exciton⁹. Fig. 2(c) gives the dimer wavefunctions for the triplet and triplet-triplet states, corresponding to the initial and final states of the ESAs, for the same Coulomb parameters and β as in Fig. 1(c) for consistency. The differences in the wavefunctions for the two sets of parameters, $U = 6.0$ eV, $\kappa = 1.8$ and $U = 7.7$ eV, $\kappa = 1.3$ are small (see Supplementary Information). The very small intensity of the triplet NIR ESA is due to the nearly 100% Frenkel character of S_0T_1 , which gives the same ESA as the monomer (to S_0T_3)²⁸. The S_0T_2 state, the final state of the very weak ESA in the NIR is overwhelmingly CT in character. The completely different characters (Frenkel versus CT) of S_0T_1 and S_0T_2 preclude strong dipole coupling between them (see Supplementary Information).

In Fig. 2(b) we have shown the calculated ESA from the ${}^1(TT)_1$ for $\beta = -0.2$ eV, where strong ESA in the visible is accompanied by ESA of moderate strength in the NIR. Interestingly, the calculated ESA energies, in both visible and NIR, as well as their relative intensities, agree very well with the PAs assigned to S_0T_1 ⁹. In analogy with the higher energy triplet states, we have labeled the final states of triplet-triplet ESA as ${}^1(TT)_2$ and ${}^1(TT)_3$, respectively, in Fig. 2(c). The complete ${}^1(TT)_1$ wavefunction, in addition to containing the product state $T_1 \otimes T_1$, has significant contributions from CT single excitations. and double

excitations that are products of T_1 and a higher energy triplet. The CT character of ${}^1(TT)_1$ is more than an order of magnitude larger than that of S_0T_1 . The partial CT character is expected within Eq. 1, since the purely $T_1 \otimes T_1$ state is reached from the ground state by two consecutive CT processes in opposite directions^{15,19,45}. Further, for the hypothetical linear polyene with fictitiously large bond alternation it has been shown that for $E(S_1) \sim E({}^1(TT)_1)$, the triplet-triplet state is a strong admixture of both $T_1 \otimes T_1$ and CT^{45,46}. Thus, the CT presence in ${}^1(TT)_1$ is simply a result of this near resonance in pentacene.

It becomes evident that CT contributions to the intial state is necessary for absorption in the IR. Within the rigid herringbone structure, the highly localized S_0T_1 has nearly vanishing CT character, and hence nearly vanishing ESA in the NIR (see Supplementary Information section IV). This result presents us with a conundrum. Either the experimental transient absorption spectra⁹ are indicating the formation of ${}^1(TT)_1$ only and not free triplets, or the triplets that absorb in the NIR are different in character from S_0T_1 of the rigid herringbone.

Local distortion, strongly coupled dimer and ESA spectra.

In the following we continue to assume that SF is efficient in pentacene. Since this necessarily requires long lasting PA both in the visible and NIR from S_0T_1 , we study the condition necessary for such triplet PA. We have calculated the ESA for the pentacene dimer with the locally distorted structure shown in the inset of Fig. 3(a). We have assumed that the dimer molecules undergo rotations and translations subsequent to photoexcitation, giving face-to-face stacking as originally suggested by Marciniak *et al.*⁷ (see Supplementary Information for details). Similar assumption has been made recently to explain excimer formation in concentrated solution¹³. We have assumed an idealized eclipsed geometry *for the sake of illustration only*. Our goal is simply to demonstrate from a model calculation that enhanced CT, driven by photoinduced change of the lattice locally, can give ESA seen experimentally. Computational results for more realistic geometries, also with enhanced CT, are presented in the Supplementary Information, where we show that the order of magnitude enhancement of $S_0T_1 \rightarrow S_0T_2$ ESA persists in these cases. It is conceivable that the local distortion follows the photogeneration of ${}^1(TT)_1$, rather than S_0S_1 , because of the completely bimolecular character of the former. Theoretical calculations have suggested that the energy barrier due to lattice strain prevents the rotations from occurring^{16,17}. Note, however, that (a) these calculations were for the S_0S_1 state only, and (b) the electronic stabilization and molecular

rotation are co-operative effects; unless the calculated electronic wavefunctions had significant CT character to begin with, calculated rotation-induced stabilization of excited states would be far too small. Whether the particular local distortion of the inset of Fig. 3(a) actually occurs or not is outside the scope of the PPP Hamiltonian, and to an extent even irrelevant (see below).

The calculated triplet ESAs for the distorted dimer (see Fig. 3(a)) show increases in oscillator strength in the NIR, by an order of magnitude relative to Fig. 2(a). Fig. 3(b) shows the calculated triplet ESAs for both $\beta = -0.2$ and -0.3 eV. Fig. 3(c) shows the calculated ESA from the ${}^1(\text{TT})_1$ now, which is largely unchanged from that in Fig. 2(b). The calculated ESA wavelengths compare very favorably with the PAs observed in experiments⁹. Fig. 3(d) shows the dominant contributions to all relevant wavefunctions. As anticipated, there is an order of magnitude increase in the CT character of $S_0 T_1$. The change in the final state of the NIR ESA, $S_0 T_2$, is insignificant. The NIR triplet ESA has an origin different from other ESAs in this wavelength and requires significant CT character in $S_0 T_1$ ⁴⁴. The triplet-triplet ESAs show a small relatively insignificant redshift and little change in intensities.

Discussions.

In conclusion, we have presented the first theoretical calculations of ESAs from the lowest singlet and triplet excitons, and the elusive triplet-triplet state for a dimer of pentacene molecules, for both the herringbone structure and a structure with local distortion leading to dimer formation. Taken together with our wavefunction analyses, they allow integrated explanations of apparently contradictory experimental observations.

First, the CT character of the lowest singlet exciton has been a matter of debate. While we²³ and others¹⁹ find close to 50% CT contribution to this excited state, other theoretical work¹⁷ have found close to vanishing CT character. This debate cannot be resolved by comparison of theory to experimental ground state absorption spectrum alone. In contrast, the experimental observation of *two* singlet PAs in the IR^{12,13}, as opposed to a single PA expected from the monomer (see Fig. 1(d) and insert) is a convincing proof of the CT character of $S_0 S_1$. Similarly, Pensack *et al.* have argued for two PAs from the ${}^1(\text{TT})_1$ at energies very close to those assigned to the triplet exciton¹². Our calculations confirm their claim.

We now come to our most important conclusions, viz., (a) the triplet exciton in the

rigid herringbone structure is highly localized with practically no CT contribution, and therefore ESA in the NIR is extremely weak; and, (b) lattice relaxation that enhances the CT contribution to S_0T_1 is essential for observable triplet PA in the NIR. We believe that the much broader NIR triplet PA that is observed experimentally, relative to the width of the singlet PA⁹, gives indirect evidence for the CT character of S_0T_1 . As seen from Fig. 3(b), small changes in β can lead to modest but visible changes in the triplet ESA energy. Since in the real material the extent of the photoinduced enhancement of the coupling between the members of a dimer can vary substantially, especially in polycrystalline films, we anticipate a distribution of β and consequently large width of the triplet NIR PA. In the case of all other NIR PAs, a distribution in β can change the relative *intensities* of the PAs, but not their widths (see Supplementary Information section IV). The observation by Herz *et al.*, that the triplet PA in the NIR is delayed relative to the supposed triplet PA to visible, can also be explained. We speculate that initial molecular distortion follows relaxation of ${}^1(TT)_1$, driven by the electronic energy that is gained if the CT contribution to its wavefunction is enhanced. Additional distortion can occur now as the ${}^1(TT)_1$ dissociates into two triplets, with the driving force now being the electronic energy gain due to the enhanced CT contribution to each triplet. The delayed PA to S_0T_2 is then related to slow molecular motion relative to electronic transitions, while the monomerlike PA to S_0T_3 occurs immediately upon the dissociation of the ${}^1(TT)_1$. Pensack *et al.* have proposed two intermediate triplet-triplet states, a strongly bound and a partially separated pair. Whether such a scheme can be explained within our proposed scenario of of pre- and post-distortion ${}^1(TT)_1$ is an intriguing question. The partial CT character of the triplet exciton may explain its long diffusion length as well as unexpectedly small binding energy, as indicated by the highly efficient charge generation in pentacene/C₆₀ bilayer⁴⁷. We finally note that our work may also explain the paucity of materials that show efficient SF. While the thermodynamic condition $E(S_1) \geq 2 \times E(T_1)$ is necessary for efficient internal conversion to ${}^1(TT)_1$, it is not enough for the actual fission of the latter into independent triplets, which may require morphology that allows local lattice distortions leading to triplets with nonnegligible CT character. We anticipate the present work to stimulate further theoretical and experimental research along this direction.

Methods The MRSDCI calculations are done iteratively for each excited state. We begin

by constructing single, double, etc. excitations within the basis space of restricted HF basis MOs that are self-consistent solutions to the extended PPP Hamiltonian. Now at the first step of the MRSDCI a few (N_{ref}) singly and doubly excited configurations that best describe the targeted excited state are selected on the basis of a trial double-CI calculation. The second step involves the MRSDCI calculation, in which the Hamiltonian matrix consists of single and double excitations from the N_{ref} configurations themselves, thereby constructing a much larger Hamiltonian matrix, including also the most important triple and quadruple excitations. From the total number N_{total} of configurations, a new set N_{ref} of most dominant single and double excitations, whose normalized coefficients in the wavefunctions are ≥ 0.04 , are chosen, and the MRSDCI calculation is performed again. This process of updating N_{ref} and N_{total} is repeated iteratively until all configurations with coefficients ≥ 0.04 have been included in N_{ref} and numerical convergence has been achieved. In the Supplementary Information we have given the N_{ref} and N_{total} that were used to obtain our bimolecular excited states. While N_{ref} is usually of the order of a hundred, N_{total} exceeds a million for most dimer eigenstates.

The optical absorptions are calculated using the standard approach, by calculating matrix elements of the transition-dipole operator $\mu = e \sum_i \vec{r}_i n_i$, where e is the electric charge, n_i has the same meaning as in Eqs. 1-3, and \vec{r}_i gives the location of the C-atom within the dimer. Linewidth of 0.03 eV has been assumed in all our absorption calculations.

The HF basis MOs we choose are products of MOs localized on individual molecules, *i.e.*, they are obtained by ignoring H_{inter} in the initial self-consistent calculation for the dimer, but are taken into consideration in each subsequent MRSDCI iteration. This procedure allows us to explicitly identify each component of a many-body eigenstate as products of charge-neutral molecular excitations, or as CT with imbalance of charges on the two molecular fragments. Furthermore, charge-neutral excitations can be predominantly one electron - one hole, in which case they are Frenkel excitations, or two electron - two hole, which at lowest energies are triplet-triplet, as also evidenced from their energies which are at $2 \times E(S_0 T_1)$.

Acknowledgments. The authors acknowledge support from NSF-CHE-1151475, the University of Arizona's REN Faculty Exploratory Research Grant and from Arizona TRIF Photonics. The authors are grateful to Dr. A. Rao for sending the experimental data from which the experimental absorption spectrum if Fig. 1(b) was constructed.

Additional Information. the authors declare no competing financial interests

Corresponding author: S. Mazumdar, sumit@physics.arizona.edu

¹ Bruno Ehrler, Brian J. Walker, Marcus L. Böhm, Mark W.B. Wilson, Yana Vaynzof, Richard H. Friend, and Neil C. Greenham. In situ measurement of exciton energy in hybrid singlet-fission solar cells. *Nat. Commun.*, 3:1019, 2012.

² J. Lee, P. Jadhav, P. D. Reusswig, S. R. Yost, N. J. Thompson, D. N. Congreve, E. Hontz, T. Van Voorhis, and M. A. Baldo. Singlet exciton fission photovoltaics. *Acc. Chem. Res.*, 46:1300–1311, 2013.

³ B. Yoo, S. aand Domercq and B. Kippelen. Efficient thin-film organic solar cells based on pentacene/C₆₀ heterojunctions. *Appl. Phys. Lett.*, 85:5427, 2004.

⁴ Daniel N. Congreve, Jiye Lee, Nicholas J. Thompson, Eric Hontz, Shane R. Yost, Philip D. Reusswig, Matthias E. Bahlke, Sebastian Reineke, Troy Van Voorhis, and Marc A. Baldo. External quantum efficiency above 100% in a singlet-exciton-fission-based organic photovoltaic cell. *Science*, 340(6130):334–337, 2013.

⁵ C. Jundt, G. Klein, B. Sipp, J. Le Moigne, M. Joucla, and A. A. Villaey. Exciton dynamics in pentacene thin films studied by pump-probe spectroscopy. *Chem. Phys. Lett.*, 241:84–88, 1995.

⁶ V. K. Thorsmølle, R. D. Averitt, J. Demsar, D. L. Smith, S. Tretiak, R. L. Martin, X. Chi, B. K. Crone, A. P. Ramirez, and A. J. Taylor. Morphology effectively controls singlet-triplet exciton relaxation and charge transport in organic semiconductors. *Phys. Rev. Lett.*, 102:017401, 2009.

⁷ H. Marcinia, I. Pugliesi, B. Nickel, and S. Lochbrunner. Ultrafast singlet and triple dynamics in microcrystalline pentacene films. *Phys. Rev. B*, 79:235318, 2009.

⁸ W.-L. Chan, M. Ligges, A. Jialaubekov, L. Kaake, L. Miaja-Avila, and X.-Y. Zhu. Observing the multiexciton state in singlet fission and ensuing ultrafast multielectron transfer. *Science*, 334:1541–1545, 2011.

⁹ Mark W. B. Wilson, Akshay Rao, Bruno Ehrler, and Richard H. Friend. Singlet exciton fission in polycrystalline pentacene: From photophysics toward devices. *Acc. Chem. Res.*, 46(6):1330–1338, 2013.

¹⁰ J. Herz, T. Buckup, F. Paulus, J. U. Engelhart, U. H. F. Bunz, and M. Motzkus. Unveiling singlet fission mediating states in TIPS-pentacene and its AZA derivatives. *J. Phys. Chem. A*, 119:6602–6610, 2015.

¹¹ A. A. Bakulin, S. E. Morgan, T. B. Kehoe, M. W. Wilson, A. W. Chin, D. Zigmantas,

D. Egorova, and A. Rao. Real-time observation of multiexcitonic states in ultrafast singlet fission using coherent 2d electronic spectroscopy. *Nat. Chem.*, 84:195411, 2011.

¹² R. D. Pensack, E. E. Ostroumov, A. J. Tilley, S. Mazza, C. Grieco, K. J. Thorley, J. B. Asbury, D. S. Seferos, J. E. Anthony, and G. D. Scholes. Observation of two triplet-pair intermediates in singlet exciton fission. *J. Phys. Chem. Lett.*, 7:2370–2375, 2016.

¹³ B. J. Walker, A. J. Musser, D. Beljonne, and R. H. Friend. Singlet exciton fission in solution. *Nat. Chem.*, 5:1019–1024, 2013.

¹⁴ M. B. Smith and J. Michl. Singlet fission. *Chem. Rev.*, 110:6891–6936, 2010.

¹⁵ E. C. Greyson, J. Vura-Weis, J. Michl, and M. A. Ratner. Maximizing singlet fission in organic dimers: Theoretical investigation of the triplet yield in the regime of localized excitation and fast coherent electron transfer. *J. Phys. Chem. B*, 114:14168–14177, 2010.

¹⁶ T. S. Kuhlman, J. Kongsted, K. V. Mikkelsen, K. B. Møller, and T. I. Sølling. Interpretation of the ultrafast photoinduced processes in pentacene thin films. *J. Am. Chem. Soc.*, 132:3431–3439, 2010.

¹⁷ P. M. Zimmerman, F. Bell, D. Casanova, and M. Head-Gordon. Mechanism for singlet fission in pentacene and tetracene: From single exciton to two triplets. *J. Am. Chem. Soc.*, 133:19944–19952, 2011.

¹⁸ M. B. Smith and J. Michl. Recent advances in singlet fission. *Annu. Rev. Phys. Chem.*, 64:361–386, 2013.

¹⁹ D. Beljonne, H. Yamagata, J. L. Brédas, F. C. Spano, and Y. Olivier. Charge-transfer excitations steer the Davydov splitting and mediate singlet exciton fission in pentacene. *Phys. Rev. Lett.*, 110:226402, 2013.

²⁰ Wai-Lun Chan, Timothy C. Berkelbach, Makenzie R. Provorse, Nicholas R. Monahan, John R. Tritsch, Mark S. Hybertsen, David R. Reichman, Jiali Gao, and X.-Y. Zhu. The quantum coherent mechanism for singlet fission: Experiment and theory. *Acc. Chem. Res.*, 46(6):1321–1329, 2013.

²¹ Tao Zeng, Roald Hoffmann, and Nandini Ananth. The low-lying electronic states of pentacene and their roles in singlet fission. *J. Am. Chem. Soc.*, 136(15):5755–5764, 2014.

²² S. R. Yost, J. Lee, M. W. B. Wilson, T. Wu, D. P. McMahon, R. R. Parkhurst, Nicholas J. Thompson, Daniel N. Congreve, A. Rao, K. Johnson, M. Y. Sfeir, M. G. Bawendi, T. M. Swager, R. H. Friend, M. A. Baldo, and T. Van Voorhis. A transferable model for singlet-fission kinetics.

Nat. Chem., 6:492–497, 2014.

²³ Karan Aryanpour, Alok Shukla, and Sumit Mazumdar. Theory of singlet fission in polyenes, acene crystals, and covalently linked acene dimers. *J. Phys. Chem. C*, 119(13):6966–6979, 2015.

²⁴ C. E. Swenberg and N. E. Geactinov. *Organic Molecular Photophysics*, volume Vol 1. Wiley-Interscience, Hobrojen, NJ, 1973.

²⁵ Jonathan J. Burdett, David Gosztola, and Christopher J. Bardeen. The dependence of singlet exciton relaxation on excitation density and temperature in polycrystalline tetracene thin films: Kinetic evidence for a dark intermediate state and implications for singlet fission. *J. Chem. Phys.*, 135(21):214508, 2011.

²⁶ G. B. Piland, J. J. Burdett, R. J. Dillon, and C. J. Bardeen. Singlet fission: From coherences to kinetics. *J. Phys. Chem. Lett.*, 5:2312–2319, 2014.

²⁷ A. J. Musser, M. Liebel, C. Schnedermann, T. Wende, T. B. Kehoel, A. Rao, and P. Kukura. Evidence for conical intersection dynamics mediating ultrafast singlet exciton fission. *Nat. Phys.*, 11:352–357, 2015.

²⁸ C. Hellner, L. Lindqvist, and P. C. Roberge. Absorption spectrum and decay kinetics of triplet pentacene in solution, studied by flash photolysis. *J. Chem. Soc. Faraday Trans.*, 68:1928–1937, 1972.

²⁹ M. Pabst and A. Köhn. Implementation of transition moments between excited states in the approximate coupled-cluster singles and doubles model. *J. Chem. Phys.*, 129:214101, 2009.

³⁰ H. Chakraborty and A. Shukla. Theory of triplet optical absorption in oligoacenes: From naphthalene to heptacene. *J. Chem. Phys.*, 141:164301, 2014.

³¹ P. Tavan and K. Schulten. Electronic excitations in finite and infinite polyenes. *Phys. Rev. B*, 36:4337–4358, 1987.

³² R. Pariser and R.G. Parr. A semi-empirical theory of the electronic spectra and electronic structure of complex unsaturated molecules ii. *J. Chem. Phys.*, 21:767–776, 1953.

³³ J. A. Pople. Electron interaction in unsaturated hydrocarbons. *Trans. Faraday Soc.*, 49:1375–1385, 1953.

³⁴ S. Uryu. Electronic states and quantum transport in double-wall carbon nanotubes. *Phys. Rev. B*, 69:075402–1–10, 2004.

³⁵ M. Chandross and S. Mazumdar. Coulomb interactions and linear, nonlinear, and triplet absorption in poly(para-phenylenevinylene). *Phys. Rev. B*, 55:1497–1504, 1997.

³⁶ K. Ohno. Some remarks on the pariser-parr-pople method. *Theor. Chim. Acta*, 2:219–227, 1964.

³⁷ Z. Wang, H. Zhao, and S. Mazumdar. Quantitative calculations of the excitonic energy spectra of semiconducting single-walled carbon nanotubes within a π - electron model. *Phys. Rev. B*, 74:195406, 2006.

³⁸ Gergely Barcza, William Barford, Florian Gebhard, and Örs Legeza. Excited states in polydiacetylene chains: A density matrix renormalization group study. *Phys. Rev. B*, 87:245116, 2013.

³⁹ J. Burgos, M. Pope, C. E. Swenberg, and R. R. Alfano. Heterofission in pentacene-doped tetracene single crystals. *Phys.Status Solidi B*, 83:249, 1977.

⁴⁰ N. Nijegorodov, V. Ramachandran, and D. Winkoun. The dependence of the absorption and fluorescence parameters, the intersystem crossing and internal conversion rate constants on the number of rings in polyacene molecules. *Spectrochim Acta. A*, 53:1813, 1997.

⁴¹ R. B. Campbell, J. M. Robertson, and J. Trotter. The crystal and molecular structure of pentacene. *Acta. Crystallogr.*, 14:705, 1961.

⁴² S. Schiefer, M. Huth, A. Dobrinevski, and B. Nickel. Determination of the crystal structure of substrate-induced pentacene polymorphs in fiber structured thin films. *J. Am. Chem. Soc.*, 129:10316–10317, 2007.

⁴³ N. J. Hestand, H. Yamagata, Xu Bolei, Sun Dezheng, Yu Zhong, Avetik R. Harutyunyan, Gugang Chen, Hai-Lung Dai, Yi Rao, and F. C. Spano. Polarized absorption in crystalline pentacene:theory vs experiment. *J. Phys. Chem. C*, 119:22137–22147, 2015.

⁴⁴ D. Psiachos and S. Mazumdar. Correlated-electron description of the photophysics of thin films of π -conjugated polymers. *Phys. Rev. B*, 79:155106, 2009.

⁴⁵ M. Chandross, Y. Shimo, and S. Mazumdar. Diagrammatic exciton-basis valence-bond theory of linear polyenes. *Phys. Rev. B*, 59:4822–4838, 1999.

⁴⁶ Karan Aryanpour, Tirthankar Dutta, Uyen Huynh, Zeev Valy Vardeny, and Sumit Mazumdar. Theory of primary photoexcitations in donor-acceptor copolymers. *Phys. Rev. Lett.*, 115:267401, 2015.

⁴⁷ A. Rao, M. W. B. Wilson, J. M. Hodgkiss, S. Albert-Seifried, H. Bässler, and R H. Friend. Exciton fission and charge generation via triplet excitons in pentacene/C₆₀ bilayers. *J. Am. Chem. Soc.*, 132:12698–12703, 2010.

Figure Captions

Figure 1 (a). The herringbone structure of the pentacene. The lattice parameters were taken from references 41,42. All calculations are for the dimer indicated in the figure. (b) Calculated absorption spectra, superimposed on the experimental low temperature absorption spectrum of pentacene film (from reference 9). (c) The dominant contributions to the normalized singlet excited states of the dimer in the pentacene unit cell, for $U = 6.0$ eV, $\kappa = 1.8$, $\beta = -0.2$ eV. Only the frontier orbitals HOMO and HOMO-1 (red), and LUMO and LUMO + 1 (blue) and their occupancies are shown. The bonds represent spin-singlet superpositions of single excitations. The double excitation indicated includes the total normalized contribution by all $T_1 \otimes T_1$ configurations. The last column gives the overall CT contributions to the wavefunctions. The three excited states to which ground state absorption occurs are all labeled S_0S_1 , so that the final states observed as transient PAs could be labeled S_0S_2 and S_0S_3 , respectively, for the purpose of being consistent with the triplet and triplet-triplet nomenclature. (d) Calculated ESA spectrum from the lowest S_0S_1 in the IR. The inset show the calculated singlet ESA for the monomer, where a single ESA occurs in the IR. Experimental observation of two PAs in the IR is clear signature of strong CT contribution to S_0S_1 (see text).

Figure 2. Calculated triplet (a), and triplet-triplet (b) ESA spectra for pentacene in the herringbone structure, for $U = 7.7$ eV, $\kappa = 1.3$ (see text). Note that the scales along the y-axes in (a) and (b) are very different; the NIR absorption in (b) is an order of magnitude stronger than in (a) (see also Fig. 3(a)). (c) The dominant contributions to the normalized triplet and triplet-triplet wavefunctions, for $U = 6.0$ eV, $\kappa = 1.8$. The arrows represent spin triplet bonds, with equal admixtures of $S_z = \pm 1$ and 0. Note the one-to-one correspondence between the ESA from S_0T_1 to S_0T_3 , and from ${}^1(TT)_1$ to ${}^1(TT)_3$, which occur in the visible. The weak NIR triplet ESA is to be anticipated from the extremely weak CT character of S_0T_1 ; the much stronger absorption here in (c) is due to the order of magnitude larger CT contribution to ${}^1(TT)_1$.

Figure 3(a). Calculated triplet ESA for $U = 7.7$ eV, $\kappa = 1.3$ and $\beta = -0.2$ eV (green solid curve), for the distorted lattice of the inset, where the two molecules constituting the dimer

are assumed to undergo rotation giving a the face-to-face structure that has also brought the molecules closer (see Supplementary Information). The triplet ESA for the herringbone structure (dashed red curve) has been included for comparison. Figure 3(b). Calculated triplet ESAs, for $\beta = -0.2$ as well as -0.3 eV. (c) Same as in Fig. 2(b) for $\beta = -0.2$ eV, and the distorted lattice. (d) Same as in Figure 2(c), with the same molecular parameters, for the rotated structure. Note the large increase in the CT character of $S_0 T_1$.

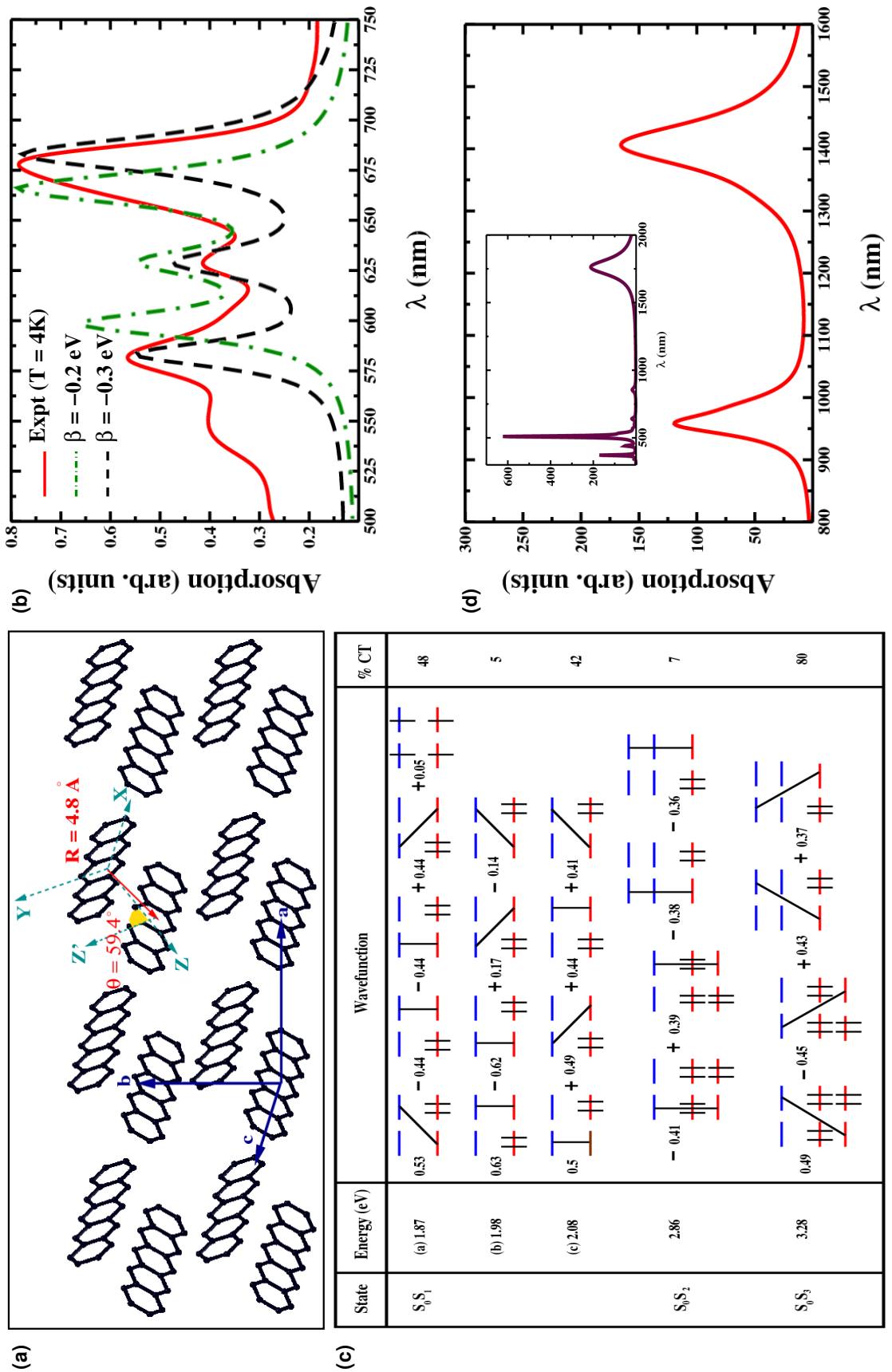


FIG. 1: Figure 1

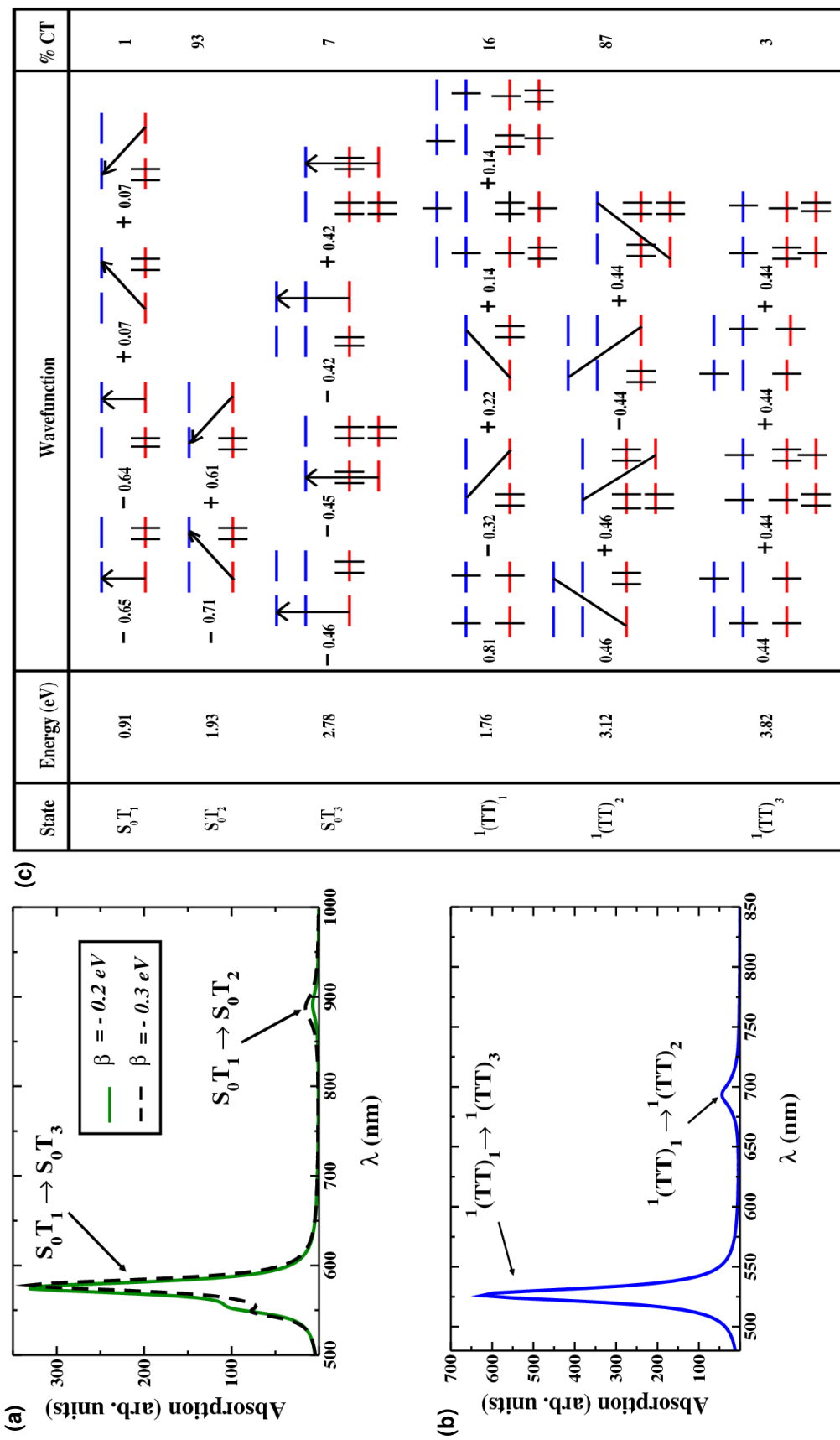


FIG. 2: Figure 2

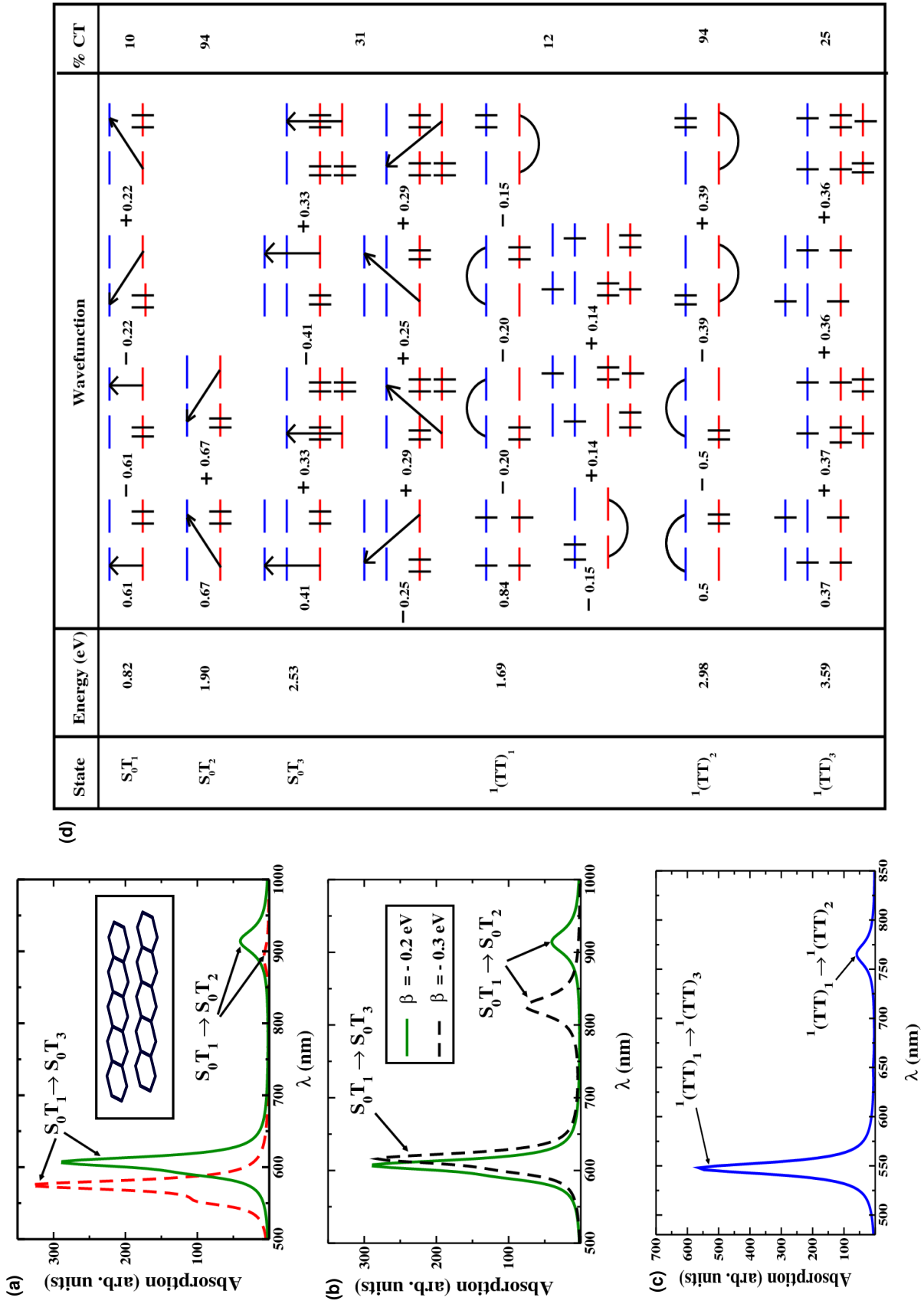


FIG. 3: Figure 3